Use of X-Ray Computed Microtomography to Understand Why Gels Reduce Permeability to Water More Than That to Oil

R. S. Seright[*], New Mexico Petroleum Recovery Research Center
J. Liang, Idaho National Engineering and Environmental Laboratory
W. Brent Lindquist, State University of New York at Stony Brook
John H. Dunsmuir, ExxonMobil Research & Engineering Company

Abstract

X-ray computed microtomography was used to investigate why gels reduce permeability to water more than that to oil in strongly water-wet Berea sandstone. We studied a Cr(III)-acetate-HPAM gel that reduced permeability to water by a factor 80 to 90 times more than that to oil. In Berea, the gel caused disproportionate permeability reduction by trapping substantial volumes of oil that remained immobile during water flooding. With this high trapped oil saturation, water was forced to flow through narrow films, through the smallest pores, and through the gel itself. In contrast, during oil flooding, oil pathways remained relatively free from constriction by the gel.

Keywords: X-ray computed microtomography, disproportionate permeability reduction.

1. Introduction

Many polymers and gels can reduce the permeability to water more than that to oil or gas (Al-Sharji 1999, Liang 1992, Liang 1995, Seright 2001a, Willhite 2000, Zaitoun 1991, Zaitoun 1998). This property is critical to the success of water-shutoff treatments in production wells if hydrocarbon-productive zones cannot be protected during polymer or gelant placement (Liang 1993, Seright 1993). However, the magnitude of the effect has been unpredictable from one application to the next. Presumably, the effect would be more predictable and controllable if we understood why the phenomenon occurs. Although many mechanisms have been considered, the underlying cause of the disproportionate permeability reduction remains elusive.

In this paper, we describe imaging experiments using high-resolution computed X-ray microtomography (XMT) to compare the oil and water pathways and fluid distributions before and after gel treatment. The current generation of synchrotron-based XMT scanners provide the ability to obtain three-dimensional pore-level images of rock samples with a spatial resolution on the order of micrometers. For this study, we used the ExxonMobil beamline X2-B at the National Synchrotron Light Source (Dunsmuir 1991, Flannery 1987). X2-B is a dedicated XMT imaging facility capable of producing continuous registered stacks of 2048 x 2048 x 1024 14-bit three-dimensional images of X-ray linear attenuation coefficients at energies tunable from 8 to 40 keV. The highly collimated synchrotron X-rays permit the reconstruction of a three-dimensional image from two-dimensional projections taken at uniformly spaced angles between 0 and 180 degrees. X2-B converts the pattern X-rays transmitted by the specimen (projections) to a visible light image using a thin single crystal of CsI(Na). This image was magnified by an optical microscope objective onto a 1024x1024 charge coupled device (CCD). Using Fourier methods,

---

* Corresponding author: fax 505-835-6031. email randy@prrc.nmt.edu

the set of angular projections at each row of pixels in the CCD was used to reconstruct the cross-sectional slice at that row. These slices were stacked to form the three-dimensional image. In this work, a 5X microscope objective was used to provide a pixel size of 4.1 μm and a 4.1-mm field of view. Since part of the core was outside the imaged area, a profile extension method was used to suppress edge artifacts.

Several authors used XMT to characterize the microscopic structure of porous media (Coles 1996, Hazlett 1996, Zhou 2000). For a 15-darcy sandstone, Coles (1998) found a mean tortuosity of 2.7, with a range from 1.5 to 4.5. Along a 2.2-mm-long section of this core, porosity varied only a few percent around the average value (26.4%). After oil flooding, this core was water flooded to a water saturation of 25.1%. Interestingly, large variations in water saturation were observed along the 2.2-mm-long section—ranging from 12% to 39%. A three-dimensional view showed the non-wetting phase (water in this case) to exist as large ganglia (blobs of non-wetting phase that extend over multiple pores—often exhibiting a branched structure).

Using XMT data, Lindquist (2000) extensively characterized pore and throat size distributions for Fontainebleau sandstones. As core porosity increased from 7.5% to 22%, the average pore coordination number increased from 3.4 to 3.8, the average channel length decreased from 200 to 130 µm, the average throat area increased from 1,600 to 2,200 μm^2, and the average pore volume remained fairly constant at around 0.0004 mm^3. The average aspect ratio (effective average pore radius/effective average throat radius) was around 2.

2. Experimental Materials

We performed two sets of imaging experiments using strongly water-wet Berea sandstone cores. The Berea cores had permeabilities of ~0.47 darcys and porosities of 22%. (Consistent porosity values were determined from both image analyses and conventional mass balance measurements.) The cores were 6.5 mm in diameter and 30 mm in length, with an intermediate pressure tap 6 mm from the inlet face. Our scans focused on a segment of the core that was 6.5 mm in diameter and 3.25 mm in length. To avoid end effects, the scanned segment was located about half way between the inlet and outlet faces. The brine used during the water floods contained 1% NaCl and 0.1% $CaCl_2$. A hexadecane mixture was used during the oil floods. To increase the image contrast between the brine and oil phases, hexadecane was doped with 10% w/w iodohexadecane in our first set of experiments in Berea and with 15% w/w bromohexadecane in the second set. All experiments occurred at room temperature. The gelant used in these experiments contained 0.5% Alcoflood 935 HPAM (molecular weight $\approx 5 \times 10^6$ daltons; degree of hydrolysis 5% to 10%), 0.0417% Cr(III) acetate, 1% NaCl, and 0.1% $CaCl_2$. The gelant viscosity at room temperature was 20 cp. The viscosities were 1.0 cp for brine (without polymer), 3.3 cp for the hexadecane/iodohexadecane mixture, and 3.6 cp for the hexadecane/bromohexadecane mixture.

3. Core Characterization

Three-dimensional scans were performed after a gelant flood and after oil and water floods both before and after gel placement. (Images were acquired at saturation endpoints.) All floods in a given set of experiments were conducted without removing the core from the sample stand so that the images could be compared directly. For each scan the image was cropped into a 2.97 mm × 2.97 mm × 2.1 mm rectangular block (the images were 725x725x512 voxels at 4.1

µm/voxel) to remove artifacts caused by those parts of the core that did not remain within the field of view through all 180 degrees of sample rotation. Image analyses were performed using a software package called 3DMA—a statistical analysis tool that correlates saturations with geometry. This software is capable of measuring distributions of pore size, pore-body/pore-throat aspect ratio, and coordination number of a porous rock using our three-dimensional images. The methods used to make these characterizations are described by Lindquist (2000).

3.1. Pore sizes

The imaged volumes included 1,736 pores for the first Berea core and 1,721 pores for the second core. Distributions of pore volumes, aspect ratios, and coordination numbers for the first core are shown in Figure 1. For the pore volumes, the *y*-axis plots the percent of the total void volume that existed in pores with a given size (indicated on the *x*-axis). The peak in the pore volume occurred at an effective pore radius (assuming spherical pores) of about 50 µm (0.0005 mm^3) for the first Berea core. The average nodal pore volumes were similar to those found by Lindquist (2000) for Fontainebleau sandstones (~0.0004 mm^3). Although many pores existed with volumes less than 0.0001 mm^3, their contribution to the total void volume was small.
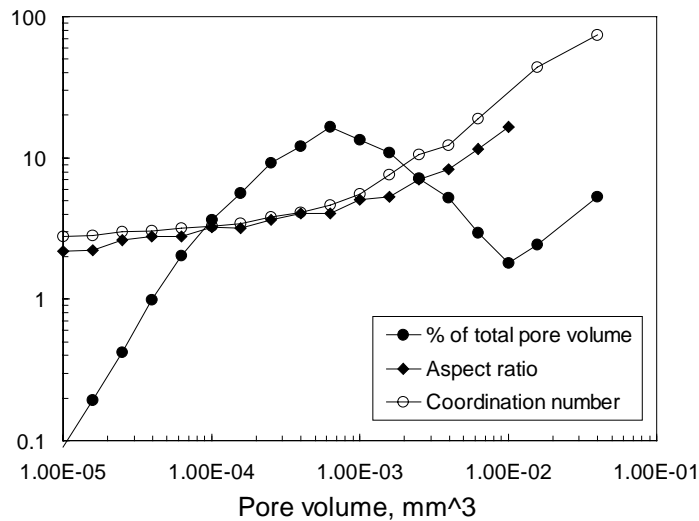

Figure 1—Distribution of pore volumes, aspect ratios, and coordination numbers for Berea.

3.2. Aspect Ratios

The distribution of aspect ratios (effective pore radius/effective throat radius) are also shown in Figure 1. (The effective pore radius assumed that the pore was spherical. The effective throat radius assumed that the throat area was circular.) The *y*-axis plots the average aspect ratio in pores with a given size (indicated on the *x*-axis). The average aspect ratio was 4.0/1. As pore volume increased from 10^{-5} mm^3 (effective pore radius ~13 µm) to 0.002 mm^3 (effective pore radius ~78 µm), the average aspect ratio increased steadily from 2 to 6. Aspect ratios jumped sharply for the few largest pores. For a given pore size, a wide range of aspect ratios were noted. At a given pore size, the standard deviation (of aspect ratios) was typically 65% of the mean value. The average throat area was 1,330 µm^2 for the first Berea core. This value was generally

lower than the average throat areas reported for Fontainebleau sandstones (1,600 to 2,200 μm^2—from Lindquist 2000).

3.3. Coordination Numbers

The distributions of pore coordination numbers are also shown in Figure 1. (The coordination number is the number of exits from a pore.) The y-axis plots the average coordination number in pores with a given size (indicated on the x-axis). The average coordination number was 3.9. For the smallest pores, the coordination number was around three. As the pore size increased, the coordination numbers increased. Coordination numbers up to 70 were noted for the largest pores. For a given pore size, standard deviations were typically 20% to 40% of the mean values.

4. Analyses After the Various Floods

XMT scans were performed after each flood. Fluid saturations and permeabilities associated with the floods are listed in Table 1.

4.1. Before Gelant Injection

In the first Berea core, the first scan viewed the core with 100% brine saturation. Second, the core was flooded with ~35 core pore volumes of oil and scanned at residual water saturation. Oil invaded most pores while the residual water appeared dominantly in crevices and films between oil and the rock. The residual water saturation, S_{wr}, was 24.7% (Table 1), and the endpoint relative permeability to oil (relative to the absolute permeability), k_{ro}, was 0.82. Third, the core was flooded with water (~70 core pore volumes) and scanned at residual oil saturation. The residual oil occupied the centers of the pores while water formed a film around the residual oil. The residual oil saturation, S_{or}, was 43.5% (i.e., 100%-56.5%, from Table 1), and the endpoint relative permeability to water, k_{rw}, was 0.16. These findings are qualitatively consistent with expectations in a strongly water-wet rock.

Table 1—Permeabilities, fluid saturations, and residual resistance factors.

	1st Berea core	2nd Berea core
Permeability, darcys	0.47	0.48
Porosity, %	22	22
S_w at 1st S_{wr}, %	24.7	37.3
k_{ro} at 1st S_{wr}	0.82	0.79
S_w at 1st S_{or}, %	56.5	56.8
k_{rw} at 1st S_{or}	0.16	0.18
S_w at 2nd S_{wr}, %		34.3
k_{ro} at 2nd S_{wr}		0.78
S_w at 1st S_{or} after gel, %	47.7	
S_w at S_{wr} after gel, %	29.0	
F_{rro}	15	
S_w at 2nd S_{or} after gel, %	21.3	
F_{rrw}	1,220	
F_{rrw} / F_{rro}	81	

Using the 3DMA software, detailed analyses were performed using the complete three-dimensional images. The distributions of water and oil saturations were determined as a function of pore size. In Figure 2, the solid symbols show the distribution of water saturations (S_w) at S_{wr} before gel placement. (In this figure and in Figure 6, average saturations for a given pore size are reported.) The open symbols show the distribution of water saturations at S_{or} before gel placement. (Of course, at any condition, the oil saturation is equal to 100% minus the water saturation.) As mentioned, the overall average S_{wr} was 24.7% for the first Berea core. This number was consistent with S_{wr} values measured using mass balances in this strongly water-wet Berea sandstone. As expected at S_{wr}, the water saturation generally increased with decreased pore size (solid circles in Figure 2). A broad minimum in water saturation was noted around 0.002 mm^3, and a local maximum was observed around 0.01 mm^3. For a strongly water-wet porous medium, one might have expected the water saturation to approach 100% for the smallest pores. Instead, the water saturation in the smallest pores averaged 60%. A calculation using the Laplace equation confirmed that oil should be able to enter the smallest pores in our Berea cores. Specifically, to enter the smallest pore throats (~7 μm radius), a capillary pressure around 1 psi was needed. This value was much lower than the 17 psi (pressure drop across the core) that was applied during our flooding experiments. The behavior of S_w versus pore size was confirmed during an imaging experiment in a second Berea core (solid squares in Figure 2). This experiment included a second oil flood (following an intervening water flood). Results from this part of the experiment (solid triangles in Figure 2) further confirmed the above behavior and indicated minimum hysteresis during cycles of water and oil flooding before gel placement. The fluid saturations and relative permeabilities from this second Berea core (Table 1) also suggest that little hysteresis occurred during multiple flooding cycles.

As mentioned, the overall average S_{or} was 43.5% for the first Berea core. This number was significantly higher than the S_{or} values measured using mass balances in this strongly water-wet Berea sandstone (~22%). At S_{or}, the average water saturation was surprisingly insensitive to pore size (open circles in Figure 2). The above results were confirmed during imaging studies of our second core (open squares in Figure 2).
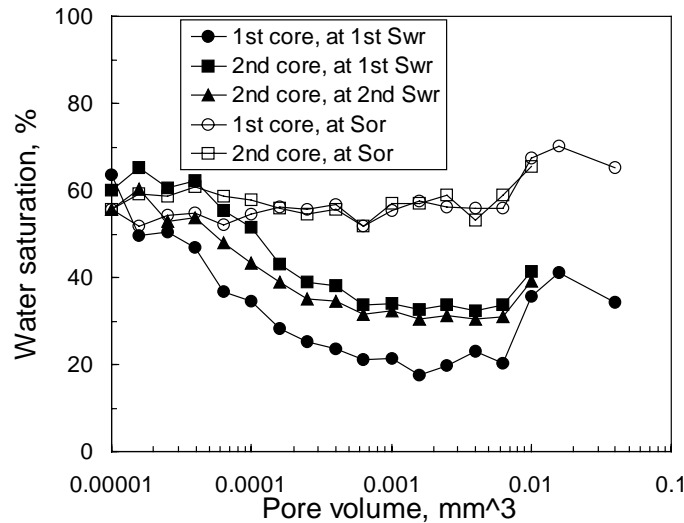

Figure 2—Water saturations at S_{wr} and S_{or} before gel placement in Berea sandstone cores.

For a given pore size, Figure 2 shows the average water saturation from a given experiment. Of course, since many pores were present for any given pore size, a range of saturations was found. A detailed examination of the data revealed that for a given pore size, the range or distribution of water saturations was quite broad, both at S_{or} and at S_{wr}.

At S_{or}, virtually all pores contained at least 20% oil and half the pores contained at least 45% oil. Assuming that spherical oil droplets were trapped in spherical pores and that the non-wetting saturation was proportional to the one-third power of droplet radius, these results indicate that virtually all pores (at S_{or}) contained oil droplets with radii that were at least 60% of the pore radius. This result is quite believable since 70% of the pores had aspect ratios greater than 2.

One feature of these XMT studies is that we can monitor the saturation differences for individual pores from one flooding stage to the next. Figures 3 and 4 plot these changes in water saturation for individual pores during oil and water flooding before gel placement. In these figures, the solid line plots the average change in water saturation for a given pore size. These solid lines are related to Figure 2. For example, the solid line in Figure 3 shows the difference between the open-circle curve (i.e., S_{or} for the first Berea core) from the solid-circle curve (i.e., S_{wr} for the first Berea core) in Figure 2. Figures 3 and 4 reveal that the average behavior results from a large variety of S_w changes that occur in individual pores. Figure 4 is particularly revealing in this regard. Recall that viewing average behavior (Figure 2) indicated that very little hysteresis occurred between the first and second S_{wr} conditions in the second Berea core. Figure 4 confirms that the saturation differences are certainly smaller than for other flooding transitions (i.e., Figure 3). Nevertheless, significant pore-level saturation differences are evident—especially for the smaller pores (in Figure 4).
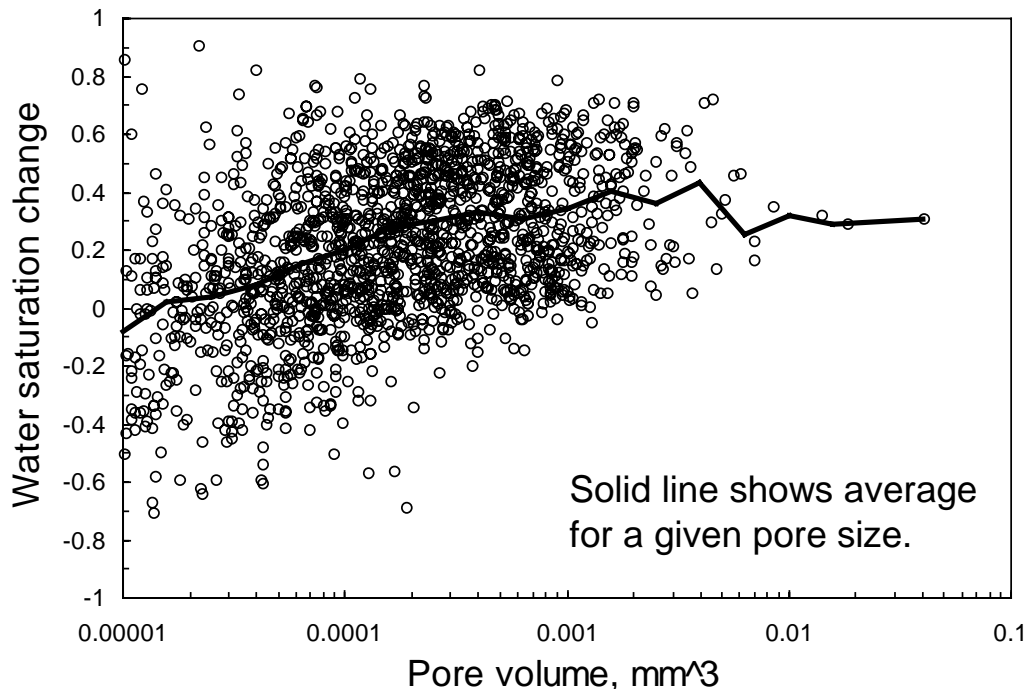

Figure 3—S_w changes from S_{wr} to S_{or} for individual pores in the first Berea core.

4.2. During Gelant Injection

After establishing a residual oil saturation in the first Berea core, the 20-cp Cr(III)-acetate-HPAM gelant (10 core pore volumes) was injected using a pressure gradient of 17 psi/ft. After gel placement, the core was shut in for twelve hours (at 60°C) and scanned (at room temperature). The gelation time for this formulation was 1 to 1.5 hours at 60°C.

Fluid saturations changed somewhat during gelant injection—specifically, average water saturations decreased slightly in the medium to large pores during gelant injection (solid line in Figure 5). Also, the overall average water saturation decreased from 56.5% to 47.7% (Table 1). On first consideration, these observations surprisingly suggest that oil was generated when gelant (containing no oil) was injected. However, the reader should recall that the imaged volume constituted only 10% of the total core volume. Conceivably, oil was displaced from upstream portions of the core during gelant injection, and this oil became trapped in the imaged volume by coincidence. Presumably, the overall oil content of the core either stayed the same or decreased slightly during gelant injection. Figure 5 confirms that many individual pores experienced saturation changes during the process of gelant injection.
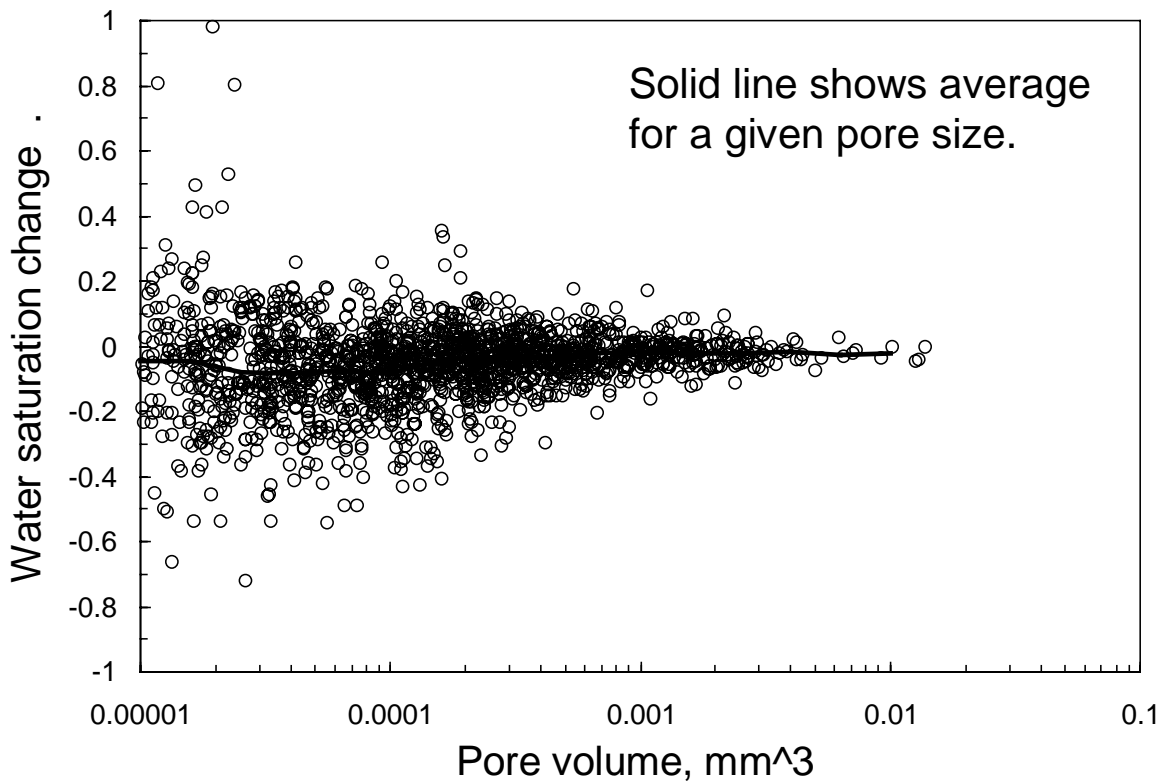

Figure 4—S_w changes from 1st S_{wr} to 2nd S_{wr} for individual pores in the 2nd Berea core.
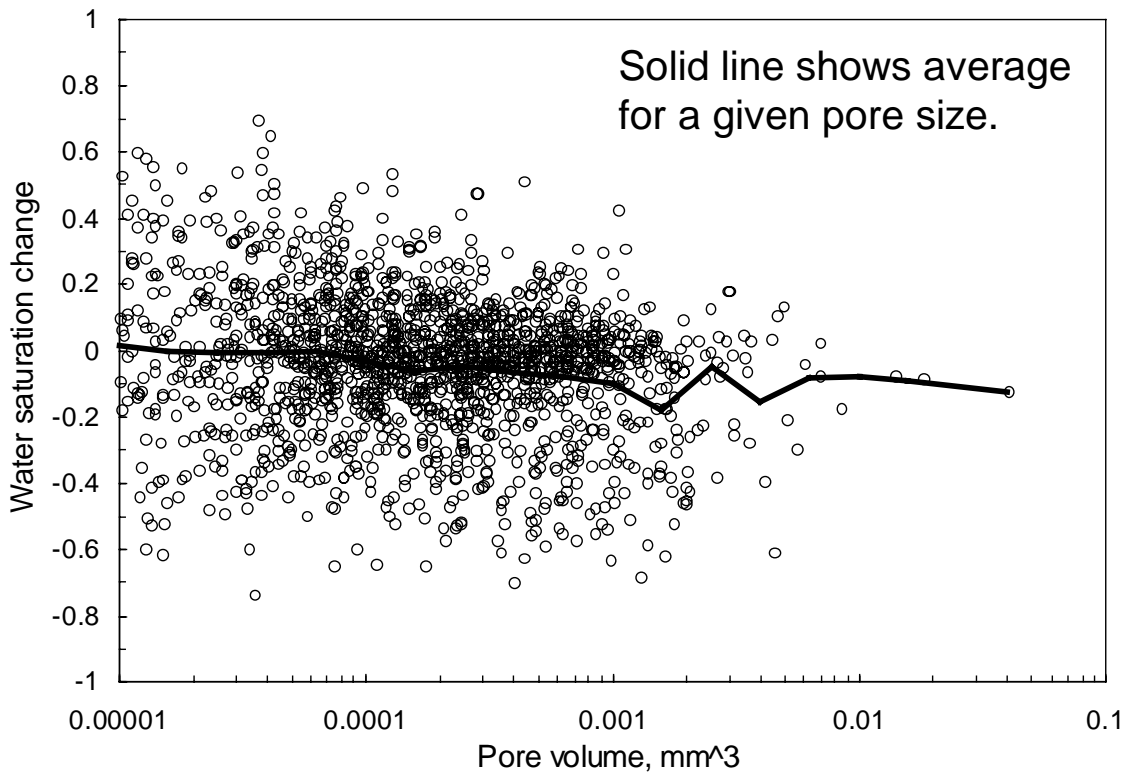
Figure 5—S_w changes during gelant injection for individual pores in the 1st Berea core.

4.3. After Gel Placement

After gel placement, oil (~20 core pore volumes) was injected to measure the oil residual resistance factor, F_{rro}—recording a value of 15. This value means that at S_{wr}, the gel reduced the permeability to oil by a factor of 15. The solid symbols in Figure 6 compare distributions of water saturations at S_{wr} before versus after gel placement. The two distributions were remarkably similar, indicating that most of the pathways that were open to oil flow before gel placement were also open to oil flow after gel placement. This result suggests that the gel occupied only a small fraction of the pore space. This suggestion is consistent with the relatively low oil residual resistance factor (i.e., 15). Tracer results from a previous experiment in a high-permeability Berea core revealed that gel with an F_{rro} value of 20 occupied less than 5% of the pore space (Liang 1992). Since the gel was placed and formed at high water saturation in the core, the result also suggests either (1) gel did not form in all the aqueous pore space (i.e., gelation was incomplete) or (2) oil flooding after gel placement moved, concentrated, or destroyed much of the gel that formed in the oil pathways.

Finally, brine (2.5 core pore volumes) was injected to measure the water residual resistance factor, F_{rrw}. The F_{rrw} value was 1,220—meaning that at S_{or}, the gel reduced the permeability to water by a factor of 1,220. This gel reduced the permeability to water 81 times more than that to oil ($F_{rrw}/F_{rro}=81$).
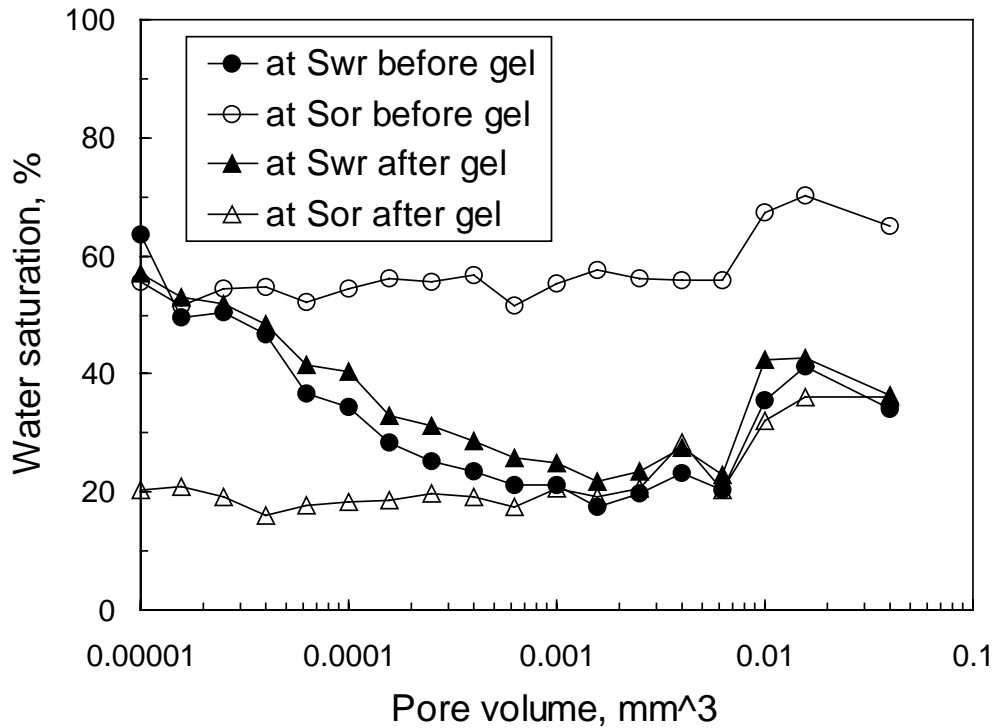
Figure 6—Effect of gel on S_{wr} and S_{or} in Berea sandstone.

At S_{or} after gel placement, water did not have access to most of the pathways that were open to oil flow after the gel treatment. The open symbols in Figure 6 compare distributions of water saturations at S_{or} before versus after gel placement. For reasons yet to be explained, water saturations in the smallest pores (<0.0005 mm^3) at S_{or} after gel placement were less than those at S_{wr}. However, more importantly (because the total pore volume was dominated by the largest pores), the distribution of water saturations in the largest pores (>0.001 mm^3) after gel placement during water flooding (open triangles) was similar to that during the previous oil floods (solid symbols in Figure 6). Therefore, the gel treatment apparently trapped substantial additional volumes of oil during water flooding (i.e., much higher S_{or} values). Perhaps, this result occurred because gel was strategically positioned in pore throats to increase aspect ratios. With the larger pores permanently occupied by oil, water was forced to flow through narrow films, through the smallest pores, and through the gel itself—explaining the large water residual resistance factor (i.e., 1,220). In contrast, oil pathways remained relatively free from constriction by the gel, so the oil residual resistance factor was much less (i.e., 15).

Saturation changes for individual pores during oil and water injection after gel placement are shown in Figures 7 and 8. During oil injection after gel placement, a sizeable number of pores experienced very little saturation change (Figure 7). Of course, many other pores gained in oil saturation. Very few pores gained significantly in water saturation. Figure 7 was quite similar to that associated with the transition from S_{or} to S_{wr} before gel placement (Seright 2001b).
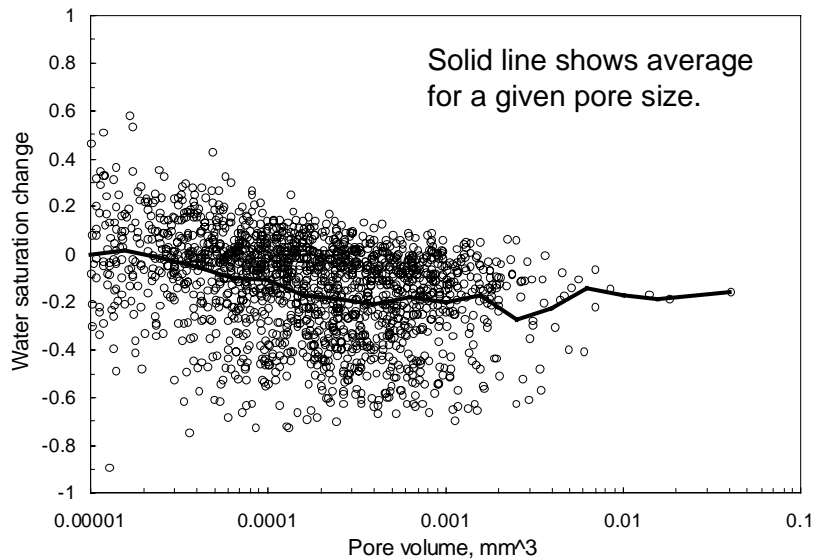
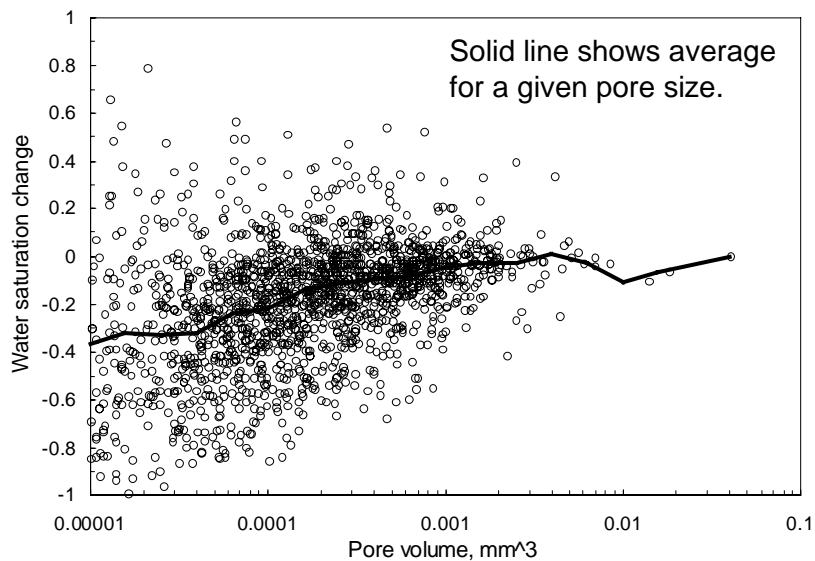Figure 7—S_w changes for individual pores in Berea during oil injection after gelation.

Figure 8—S_w changes for individual pores in Berea during water injection after gelation.

During water injection after gel placement (Figure 8), many pores also experienced only small saturation changes. Many other pores experienced significant changes, with many gaining water while others gained in oil. The scatter in Figure 8 suggests that a significant amount of saturation rearrangement occurred during water injection, but the overall saturation did not change greatly (i.e., the overall water saturation changed from 29.0% to 21.3%, from Table 1).

Figure 9 compares saturation differences for individual pores before versus after gel placement when the core was at S_{wr}. Consistent with our earlier observations, at S_{wr}, most pores appeared to have about the same saturation after gel placement as before gel placement. This

observation was most noticeable for the medium to large pores and was less valid for the smallest pores (i.e., those smaller than 10^{-4} mm^3).
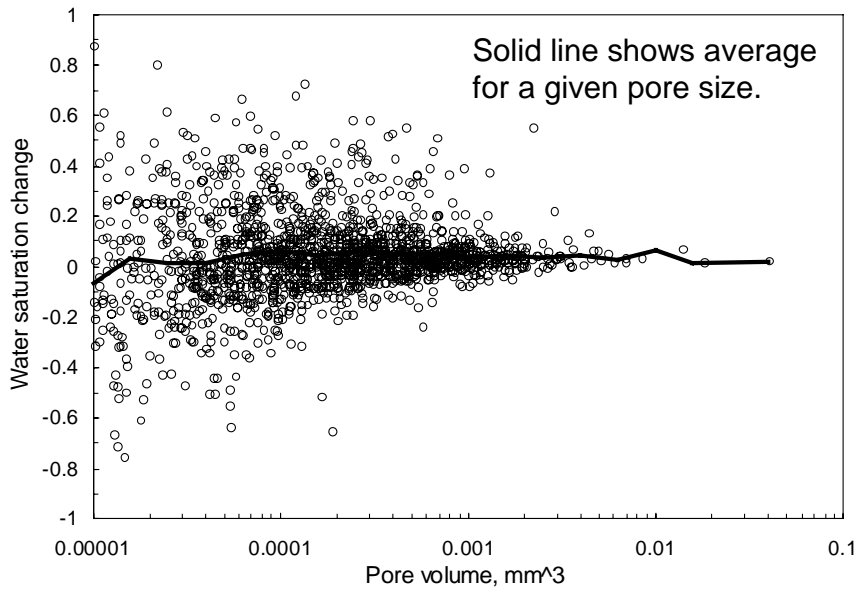

Figure 9—S_w differences for individual pores in Berea at S_{wr} before versus after gel placement.

Figure 10 compares saturation differences for individual pores before versus after gel placement when the core was at S_{or}. This figure confirms that most pores (of all sizes) contained significantly more oil at S_{or} after gel placement than before gel placement. Thus, during water injection, the gel inhibited water flow by increasing the trapped oil saturation in most pores.
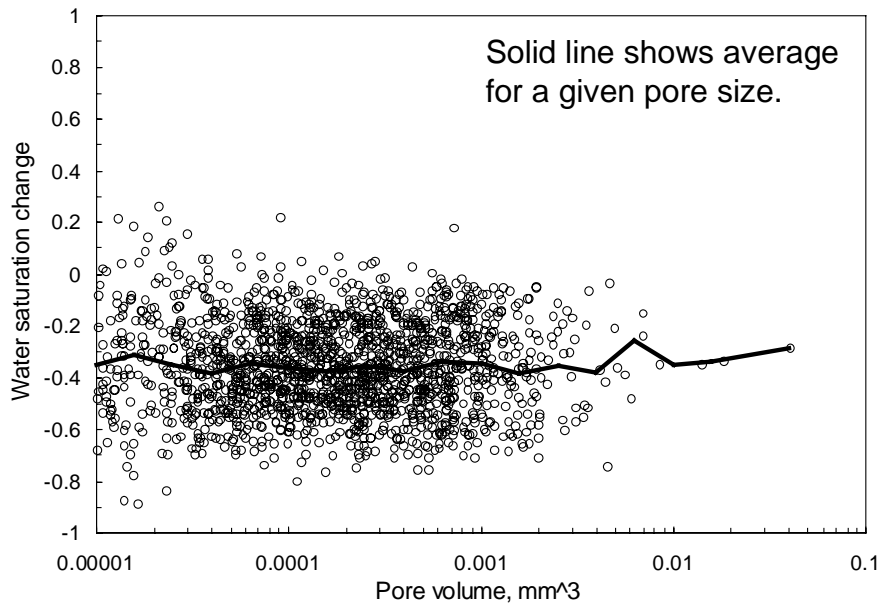

Figure 10—S_w differences for individual pores in Berea at S_{or} before versus after gel placement.

5. Relevance to Field Applications

When production wells were treated with gelants, some zones had high water saturations and high fractional water flows, while other zones had high hydrocarbon saturations and fractional flows. For the oil zones, the flooding sequence used for this paper mimics the field situation. Specifically, oil was the first fluid to flow through the gel after the treatment. Thus, the oil residual resistance factor of 15 and the mechanism for establishment of oil permeability through the gel are relevant to field applications (Liang 1993, Seright 1993). However, this is not the case for the water zones. Specifically, in water zones in field treatments, water was the first fluid to flow through the gel after gel placement—i.e., no oil flowed through the gel in the water zones. For this circumstance, our previous experience with Cr(III)-acetate-HPAM gels revealed that water residual resistance factors were ~10,000 and the gel occupied virtually all of the aqueous pore space (Liang 1992, Seright 1993). Thus, the mechanism for water permeability reduction in field applications is actually one of near-total blockage of water flow. Virtually the only means for water flow is through the gel itself (which has a permeability less than 1 mD) (Seright 1996, Seright 2001b). In contrast, in the experiments here, the mechanism of water flow was examined after oil flowed through the gel. Nevertheless, since the water residual resistance factor in these experiments was 80-90 times greater than the oil residual resistance factor, the mechanism of permeability reduction for water is of scientific interest.

6. Conclusions

X-ray computed microtomography was used to investigate why gels reduce permeability to water more than that to oil in strongly water-wet Berea sandstone. The following conclusions were reached:

1. A Cr(III)-acetate-HPAM gel reduced permeability to water by a factor 80 to 90 times more than that to oil.
2. In Berea, gel caused disproportionate permeability reduction by trapping substantial volumes of oil that remained immobile during water flooding. With this high trapped oil saturation, water was forced to flow through narrow films, through the smallest pores, and through the gel itself. In contrast, during oil flooding, oil pathways remained relatively free from constriction by the gel.

Nomenclature

F_{rr} = residual resistance factor
F_{rro} = residual resistance factor for oil
F_{rrw} = residual resistance factor for water
k_{ro} = relative permeability to oil
k_{rw} = relative permeability to water
S_{or} = residual oil saturation, %
S_w = water saturation, %
S_{wr} = residual water saturation, %

Acknowledgments

References

Al-Sharji, H.H., *et al*., 1999: "Pore-Scale Study of the Flow of Oil and Water through Polymer Gels," paper SPE 56738 presented at the 1999 SPE Annual Technical Conference and Exhibition, Houston, Oct. 3-6.

Coles, M.E., *et al.*, 1996: "Pore Level Imaging of Fluid Transport Using Synchrotron X-Ray Microtomography," paper 9628 presented at the International Symposium of the Society of Core Analysts, Montpellier, France, Sept. 8-10.

Coles, M.E., *et al*, 1998.: "Developments in Synchrotron X—Ray Microtomography with Applications to Flow in Porous Media," *SPEREE*, 288-296.

Dunsmuir, J.H., *et al*, 1991.: X—Ray Microtomography: A New Tool for the Characterization of Porous Media, paper SPE 22860 presented at the 1991 SPE Annual Technical Conference and Exhibition, Dallas, Oct. 6-9.

Flannery, B.P., *et al.*, 1987: "Three-Dimensional X—Ray Microtomography," *Science*, **237**, 1389.

Hazlett, R.D., Chen, S.Y, and Soll, W.E., 1996: "Wettability and Rate Effects on Immiscible Displacement: Lattice Boltzmann Simulation in Microtomographic Images of Reservoir Rocks," presented at the 4th International Symposium on Evaluation of Reservoir Wettability and its Effect on Oil Recovery, Montpellier, France, Sept. 11-13.

Liang, J., Sun, H., and Seright, R.S., 1992: "Reduction of Oil and Water Permeabilities Using Gels," paper SPE 24195 presented at the 1992 SPE/DOE Symposium on Enhanced Oil Recovery, Tulsa, April 22-24.

Liang, J., Lee, R.L., and Seright, R.S., 1993: "Placement of Gels in Production Wells," *SPEPF* 276-284; Transactions AIME 295.

Liang, J., Sun, H., and Seright, R.S., 1995: "Why Do Gels Reduce Water Permeability More Than Oil Permeability?" *SPERE* (Nov. 1995) 282-286.

Lindquist, W.B., *et al.*, 2000: "Pore and Throat Size Distributions Measured From Synchrotron X-Ray Tomography Images of Fountainebleau Sandstones," *J. Geophys. Research*, **105B**, 21508-21528.

Seright, R.S., Liang, J., and Sun, H., 1993: "Gel Treatments in Production Wells with Water Coning Problems," *In Situ* **17**(3) 243-272.

Seright, R.S., 1996: "Improved Techniques for Fluid Diversion In Oil Recovery," final report, DOE/BC/14880-15, U.S. DOE, 97-108.

Seright, R.S, Liang J., Lindquist, B.W., and Dunsmuir, J.H., 2001: "Characterizing Disproportionate Permeability Reduction Using Synchrotron X-Ray Computed Microtomography," paper 71508 presented at the 2001 SPE Annual Technical Conference and Exhibition, New Orleans, Sept. 30- Oct. 3.

Seright, R.S., 2001: "Using Chemicals to Optimize Conformance Control in Fractured Reservoirs," annual report (DOE/BC/15110-6), Contract No. DE-AC26-98BC15110, U.S. DOE.

Willhite, G.P., *et al.*, 2000: "Mechanisms Causing Disproportionate Permeability in Porous Media Treated With Chromium Acetate/HPAAM Gels," paper SPE 59345 presented at the 2000 SPE/DOE Improved Oil Recovery Symposium, Tulsa, April 3-5.

Zaitoun, A. and Kohler N., 1991: "Thin Polyacrylamide Gels for Water Control in High-Permeability Production Wells" paper SPE 22785 presented at the 1991 SPE Annual Technical Conference and Exhibition, Dallas, Oct. 6-9.

Zaitoun, A., Bertin, H., and Lasseux, D., 1998: "Two-Phase Flow Property Modifications by Polymer Adsorption," paper SPE 39631 presented at the 1998 SPE/DOE Improved Oil Recovery Symposium, Tulsa, April 19-22.

Zhou, M., *et al.*, 2000: "Irreducible Water Distribution in Sandstone Rock: Two-Phase Flow Simulations in CT-based Pore Network," *Phys. Chem. Earth (A),* **25**(2), 169-174.